CHAPTER IV

RESULTS AND DISCUSSION

4.1 Catalyst Characterization

This Chapter was divided into 2 main section, catalyst characterization and photocatalytic testing of 2,4-DCP. Temperature is an important effect on TiO_2 phase transformation. The as-synthesized dried sol-gel, was then tested by TG-DTA. Temperature range providing anatase phase was used as guidance for the further characterization studies. This included XRD, UV-DRS, XANES, ZP and specific surface area analysis.

4.1.1 Thermal analysis

To obtain porous structure, the organic template has to be removed. The organic template can be eliminated from the as-synthesized photocatalyst by calcinations. The TGA curve of all samples could be classified into two stages of weight losses. The first range was between 30-400°C with approximately 50% weight loss as presented in Figure 4.1(a-c) attributed to the combustion of organic templates. The second range was from 450-600°C considered to nitrate ion. It can be seen from DTA curve Figure 4.1(d-f) in which a broad endothermic peak near 100°C is due to evaporation of the physically absorbed water, and the first exothermic peak between 200 and 230°C may be attributed to phase transformation of amorphous to anatase. The last exothermic (500-600°C) inferred to the transmutation from anatase to rutile phase of TiO_2 (Zhou et al., 2006). This calcination temperature was designed at 400°C to obtain only the anatase phase of TiO_2. As a result, anatase was believed to be the most efficient photocatalyst during chemical reaction (Shah et al., 2002).

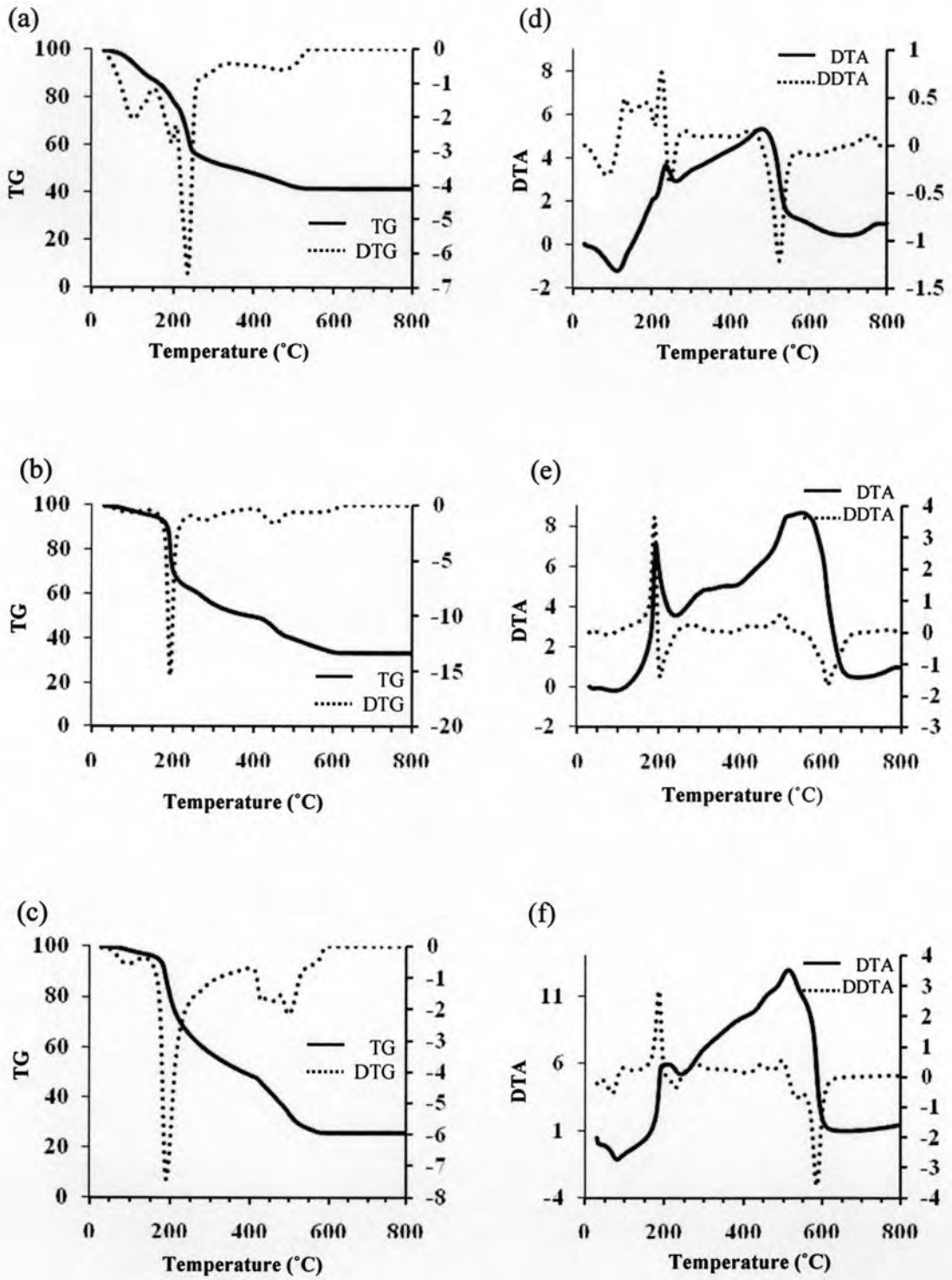

Figure 4.1 (a-c); TG/DTG curves of the different templates at 1%Fe,
(d-f); DTA/DDTA curve of the different templates at 1%Fe,
(a,d):6C, (b,e):12C, (c,f):18C type of template.

4.1.2 Structure and crystallite size

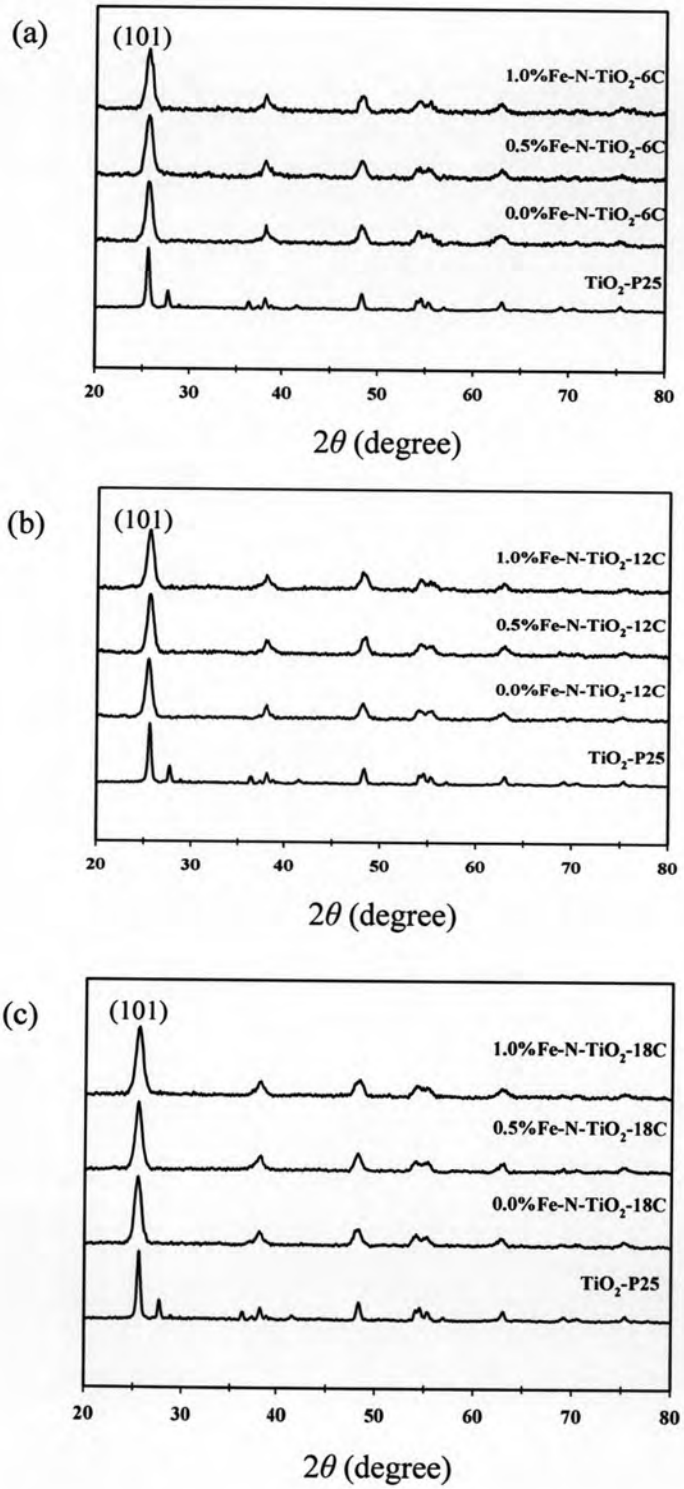

Figure 4.2 XRD patterns of TiO_2 (Degussa P25) compared with each type of template at different mol %Fe.

The XRD patterns of the photocatalysts compared with commercial TiO_2 (Degussa-P25) are shown in Figure 4.2 (a-c). The dominant peaks at 2θ about 25.2, 37.9°, 47.8°, 53.8° and 55.0° represented the indices of (101), (004), (200), (105), and (211) planes in standard JCPDS file no.21-1272. It was which conformed to the crystalline structure of anatase explained by Zhu et al., 2005. Within the detection limit of this technique, all samples consisted of anatase as the unique phase while crystalline phase containing Fe could not be observed, even at high Fe concentration. There are two reasons responsible for this. The first reason was that the concentration of Fe-doping was too low to be detected by XRD. The other was some Fe might insert into the structure of TiO_2 due to its radii of Ti^{4+} (0.68Å) and Fe^{3+} (0.64Å) ions are very similar (Zhou et al., 2006).

Table 4.1 Crystal sizes and surface areas of TiO_2 (P25) and Co-doped photocatalyst

Samples	Crystal size (nm)	BET surface area (m^2g^{-1})
TiO_2-P25	18.87	36.36
0.0Fe-N-TiO_2-6C	9.52	129.14
0.5Fe-N-TiO_2-6C	8.56	137.53
1.0Fe-N-TiO_2-6C	8.89	145.25
0.0Fe-N-TiO_2-12C	9.83	112.67
0.5Fe-N-TiO_2-12C	9.61	111.31
1.0Fe-N-TiO_2-12C	8.64	121.18
0.0Fe-N-TiO_2-18C	9.11	102.98
0.5Fe-N-TiO_2-18C	9.77	111.74
1.0Fe-N-TiO_2-18C	8.85	130.00

The crystal sizes were also determined by XRD analysis using Scherrer equation and calculated from FWHM of the anatase main peak (101). The results are tabulated in Table 4.1. The broader peaks indicated that the crystalline sizes of the samples were relatively smaller than the commercial TiO_2 (P25). Furthermore, the characteristic peaks showed that co-doped catalyst contained more of the active crystalline anatase phase than TiO_2 (P25). For the amount of Fe-loading and different types of template, they did not significantly affect the crystallite size of the catalysts.

4.1.3 Specific surface area

The specific surface areas of all studied photocatalysts are shown in Table 4.1. All photocatalysts prepared by sol-gel methods had a large surface, which were higher than the surface area of commercial TiO_2 (P25). It can be seen that with increasing Fe-doping concentration, the specific surface area of photocatalyst increased while the different types of templates did not significantly affect the surface area.

4.1.4 Light adsorption capability

The UV-vis diffuse reflectance spectra of co-doping and commercial TiO_2 (P25) are shown in Figure 4.3. The spectra showed that P25 exhibits absorption at the wavelength around 400 nm due to the intrinsic band gap of TiO_2. Every template, with the increase of Fe^{3+} doping concentration, the absorbance in visible light range (400-700 nm) clearly increase as show in Figure 4.3. The presence of Fe^{3+} in TiO_2 did not change the position of VB of TiO_2. Instead, it might introduce new energy level between VB and CB edge of TiO_2. Therefore, the absorption edges shift toward longer wavelengths for the Fe-doped TiO_2. This should come from the electronic transition from the Fe^{3+} energy level to the CB of TiO_2. This clearly indicated a decrease in the band gap energy of prepared catalysts (Tong., 2007; Zhou et al., 2006). While, with the same loading of Fe^{3+} concentration the absorbance are quite the same, and there is no effect based on the template types as show in Figure 4.4.

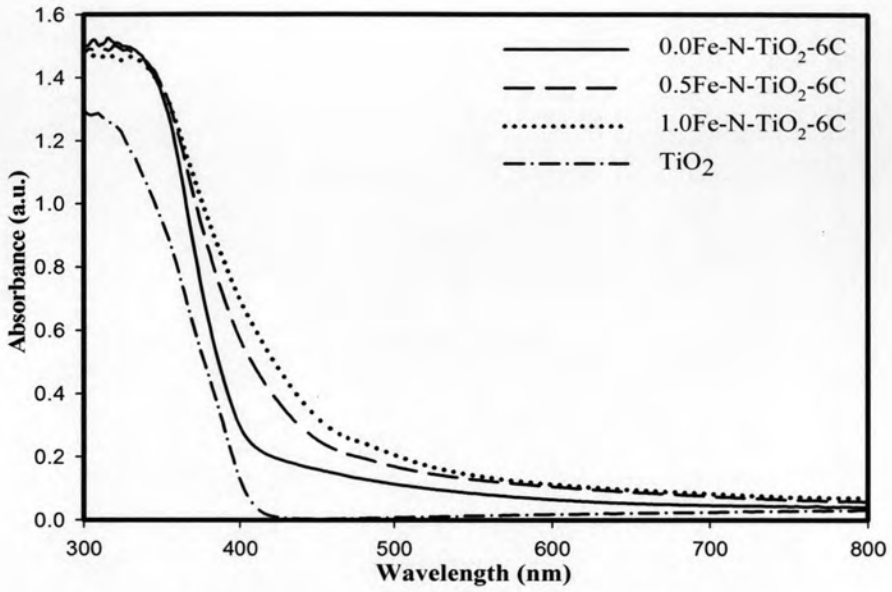

Figure 4.3 UV-DRS spectra of TiO_2-P25 compared 6C-template photcatalysts with different mol%Fe.

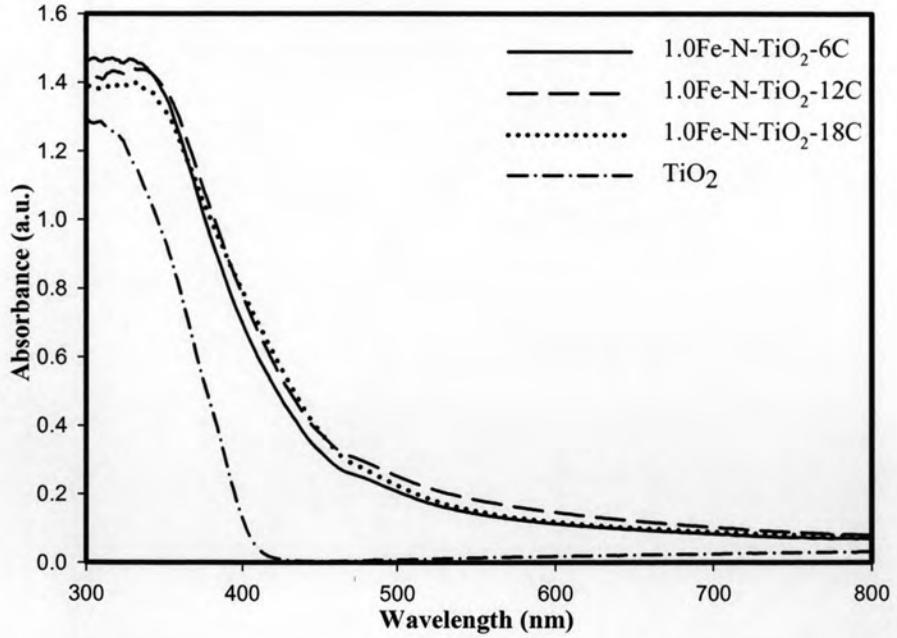

Figure 4.4 UV-DRS spectra of 1.0%Fe-N-TiO_2 with different templates.

The band gap energy (E_g) for all samples was calculated using equation 3.2. Figure 4.5-4.6 are shown the graph of $(kh\upsilon)^{1/2}$ versus photon energy ($h\upsilon$). These plots were referred to as "the Tauc plots". The linear portion of the curve extrapolating to zero gave the value of the E_g. According to the Tauc plots, the E_g of catalysts are presented in Table 4.2. The band gap energy decreased with the increasing of Fe^{3+} doping concentration (Figure 4.5). However, there is no change of E_g from catalyst prepared by different templates, as show in Figure 4.6

Table 4.2 Energy band gap of catalysts.

Mol % Fe doped	Energy band gap (E_g)		
	6C	12C	18C
0.0%Fe	2.80	2.70	2.80
0.5%Fe	2.50	2.40	2.44
1.0%Fe	2.30	2.26	2.20

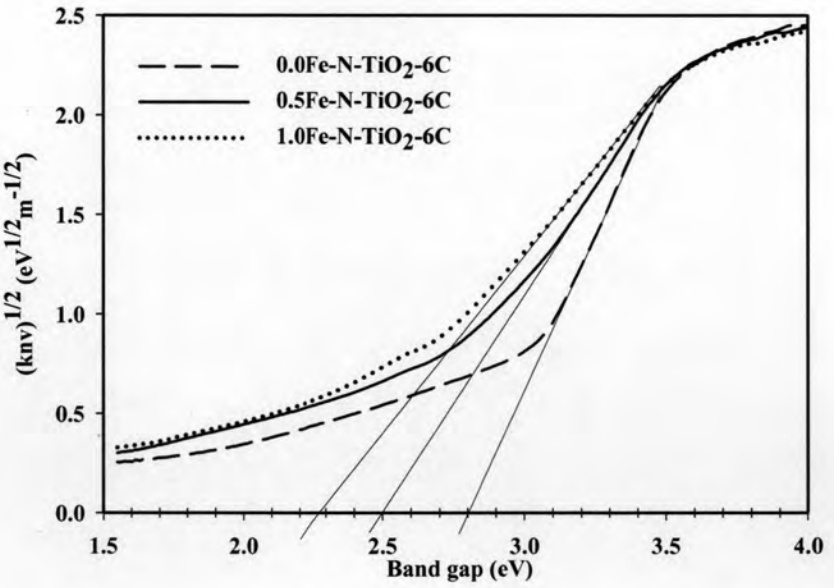

Figure 4.5 Tauc plots of 6C-template photocatalyst with different mol%Fe

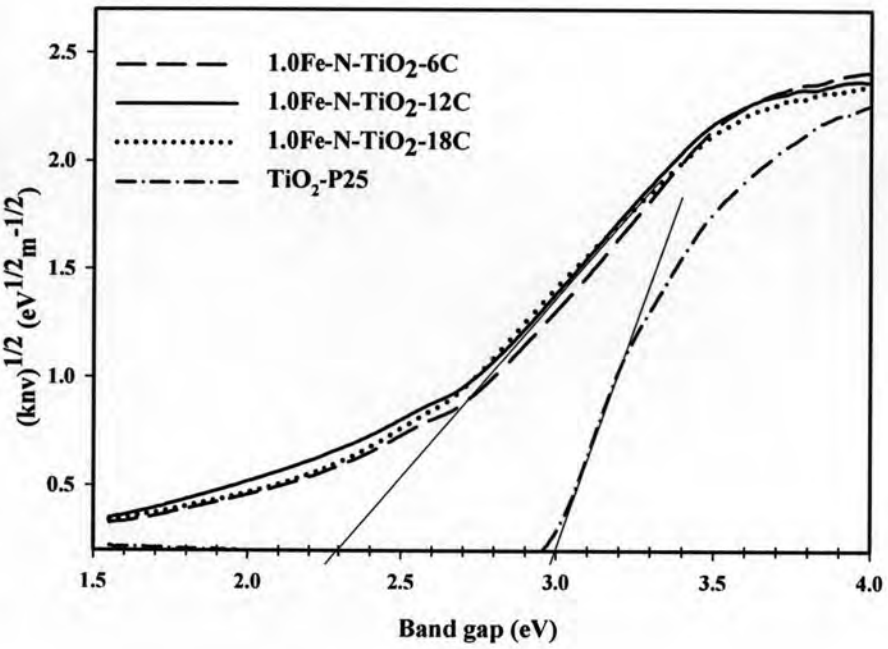

Figure 4.6 Tauc plots of TiO_2-P25 compared 1.0%Fe with different types of templates.

4.1.5 Oxidation state

XANES analysis was carried out to identify the photocatalysts's valence state of Fe and Ti. In XANES, the valence state of metal cation can be deduced from the energy shift of the pre-edge absorption, which is a small peak before the sharp rise peak in the spectrum. Figure 4.7 shows the XANES spectra of Ti K-edge of co-doped TiO_2 samples compared with commercial TiO_2 (P25) which is used as Ti^{4+} standard. The spectra confirmed that Ti species were in the form of Ti^{4+} or TiO_2 for all samples. Figure 4.8 show the XANES spectra of Fe K-edge. Fe-doped TiO_2 compared with Fe_2O_3 as a reference material. The results showed that XANES spectra had similar edge energy regardless of Fe content, which was compatible with Fe ions with +3 oxidation state (Rodriguez-Torres C.E. et al., 2008).

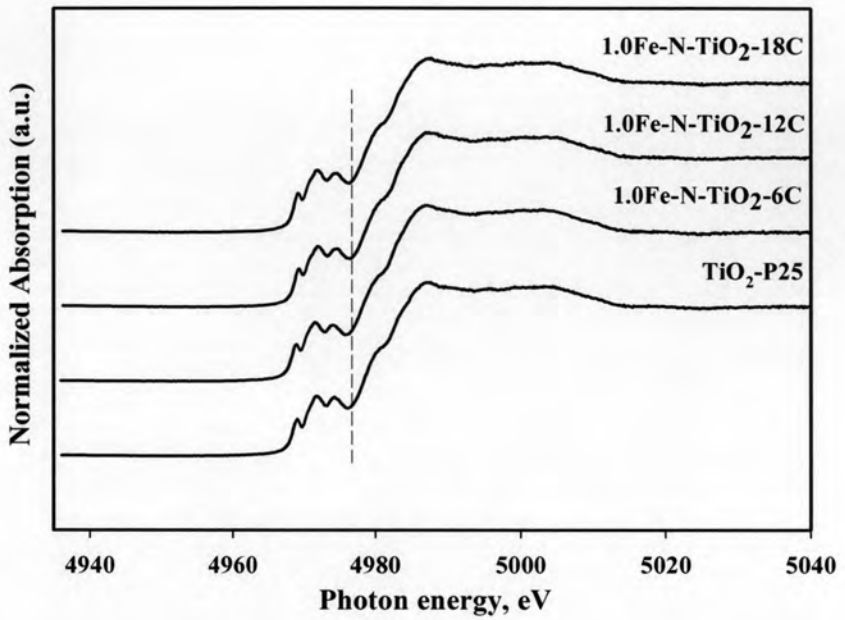

Figure 4.7 The XANES spectra (Ti K-edge) of samples with different types of templates, 1%Fe doped compared with TiO_2-P25 as references material.

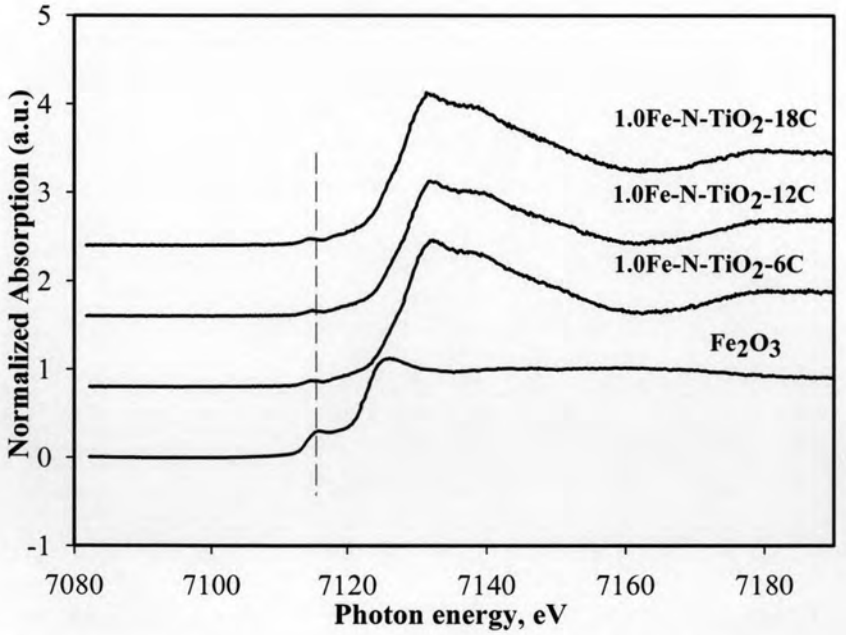

Figure 4.8 The XANES spectra of (Fe k-edge) of samples with different types of templates, 1%Fe doped compared with Fe_2O_3 as reference material.

4.1.6 Electrokinetic potential (zeta-potential) of photocatalysts surface

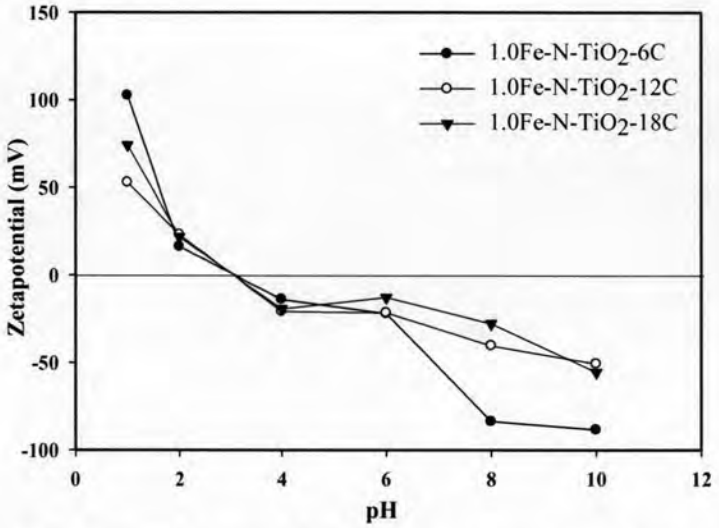

Figure 4.9 Zeta-potential of photocatalysts suspensions on pH of DI-water.

The electrokinetic potential or zeta potential of 1.0%Fe-N-TiO_2 with difference templates are shown in Figure 4.9. The point where the plot passes through zero of zeta potential is called the zero point charge (pH_{zpc}). pH_{zpc} of all photocatalysts was found at pH 3.0. When the pH value is less than pH_{zpc}, the catalyst surface contains more positive charges and more negative charge when pH value is over than pH_{zpc}. The substances formerly attached to the catalyst surface as a result of electrostatic adsorption begin to leave the catalyst under the influence of electric repulsion between the substances and the catalyst, thus lowering the oxidation/reduction rate of the reactants. Therefore, the ionic reactants are more affected by the pH of the environment due to electrostatic interaction. The pKa value of 2,4-DCP is 7.89 ($C_6H_3Cl_2OH \rightarrow C_6H_3Cl_2O^- + H^+$, pKa = 7.89). When the pH value of the solution is higher than its pKa, it exists mainly in ionic form and is more affected by the electric nature of the photocatalysts surface. It could be inferred that more 2,4-DCP could be adsorbed on catalysts surface at pH 3.0 while both of 2,4-DCP and catalyst surface are neutral. However, this pH is likely strong acid. It is difficult to improve for the future work or real wastewater treatment, while the pH limitation of industrial effluent is controlled at pH 5.5-9.0 (PCD, 1996: online). In this study the reaction was tested with pH of 5.5.

4.2 Photocatalytic testing of 2,4-DCP

4.2.1 Experimental design analysis

Box-Behnken statistical screening design was used to optimize and evaluate main effects, interaction effects, and quadratic effects to the operating conditions for maximizing the 2,4-DCP degradation. In this work, three factors Box-Behnken design having three central points with double replicate was used for exploring quadratic response surfaces. This statistical analysis was done under mol% Fe, type of template, and catalyst loading, as shown in Table 4.3

Table 4.3 Variables in the Box-Behnken Design.

Parameters	Level used		
	Low	Medium	High
Type of template	6C	12C	18C
Catalyst loading (g/L)	0.5	1.0	1.5
%Fe	0.0	0.5	1.0

Following the Box-Behnken, The total amount of experiment was designed in 30 batchs. The experiments were carried out with a 2,4-DCP initial concentration of 15 ppm at pH 5.5, for 1 h reaction time. The experimental matrix generated by the MINITAB V.15 software and the results of the model for the percentage of 2,4-DCP removed are shown in Table 4.4 The percent degradation was presented as the response term. The evaluated value at different factor level combinations was treated statistically to develop a response surface model.

Table 4.4 Box-Behnken design matrix and the response (% degradation)

Run order	Parameters			Response (% degradation)
	Type of template	Catalyst loading (g/L)	%Fe	
1	12	1.0	0.5	7.3609
2	18	0.5	0.5	3.4953
3	12	1.0	0.5	7.6608
4	6	0.5	0.5	4.3149
5	18	1.0	0.0	6.6324
6	18	0.5	0.5	4.0642
7	12	0.5	0.0	5.9742
8	12	0.5	0.0	6.4103
9	12	1.0	0.5	5.4708
10	6	1.0	0.0	8.4164
11	12	1.5	0.0	11.8855
12	18	1.0	0.0	7.5263
13	12	1.0	0.5	9.2832
14	6	1.0	1.0	8.0986
15	18	1.5	0.5	10.3175
16	12	1.5	1.0	12.5812
17	18	1.5	0.5	9.7691
18	12	1.5	1.0	12.4774
19	12	0.5	1.0	7.7338
20	6	0.5	0.5	4.8098
21	18	1.0	1.0	9.1165
22	18	1.0	1.0	8.2457
23	12	0.5	1.0	5.5648
24	6	1.5	0.5	12.1938
25	12	1.0	0.5	8.3567
26	12	1.0	0.5	8.8999
27	6	1.5	0.5	11.2135
28	6	1.0	1.0	8.1828
29	12	1.5	0.0	13.4477
30	6	1.0	0.0	9.5559

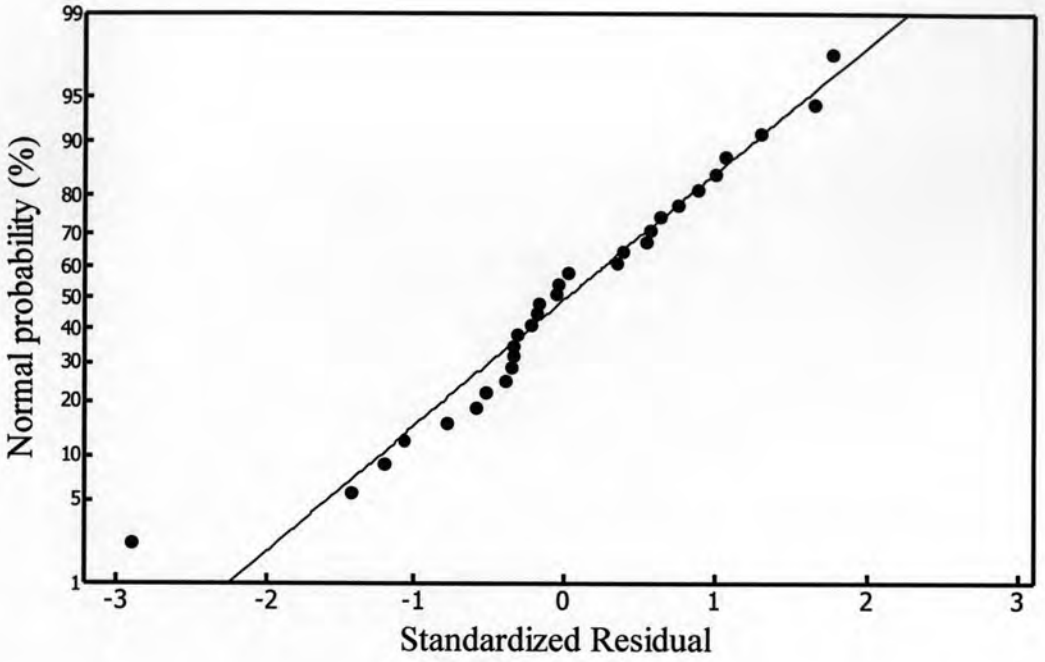

Figure 4.10 Normal probability plots

Normally, the model has to confirm that it gives sufficient approximation to the actual results. Normal probability plot of the residual for percentage degradation is used to check the goodness of the model, as shown in Figure 4.10 It can be seen that the residuals are falling on a straight line, which means that the errors are normally distributed. It can be confirmed that the predicted values are in good agreement with the observed values. The plot of standardized residuals against fitted value (predicted response) is showed in Figure 4.11. The plot of residuals versus fitted values shows randomly scatter of residuals on both sides of zero line. It could imply that the variance of original observations is constant for all values of the response. This plot was the one that can confirm the model sufficient to estimate the degradation efficiency of 2,4-DCP in this studied range.

Moreover, the standardized residual for the batch run (Figure 4.12) was used to confirm the approximation of the fitted model whether it was in a good agreement with the data. Since the values from this experiment were in the interval of ± 3.50, it was reasonable to be accepted.

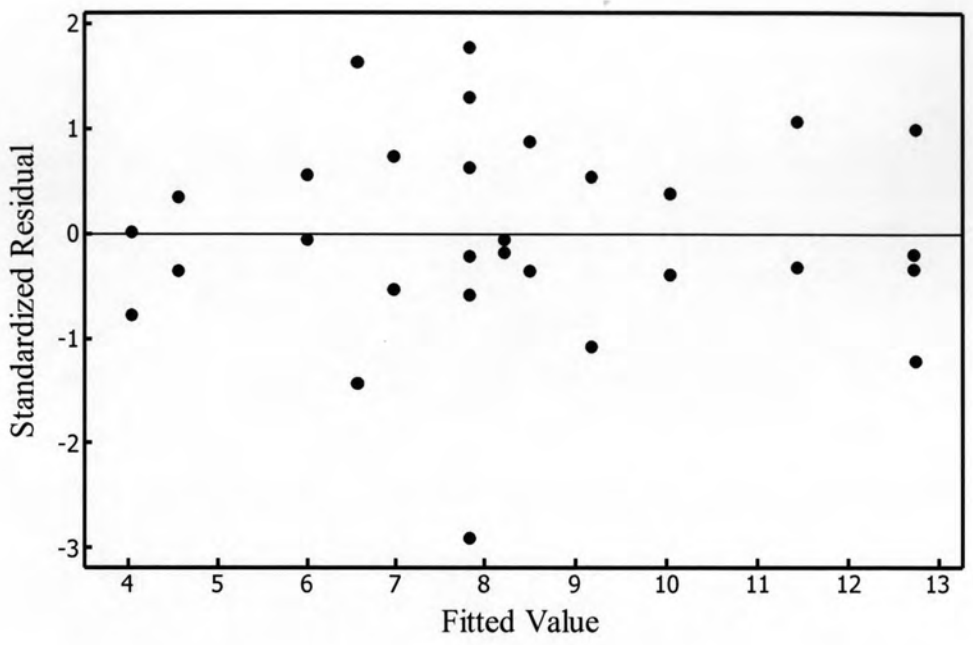

Figure 4.11 Plot of residual versus fitted values (predicted values)

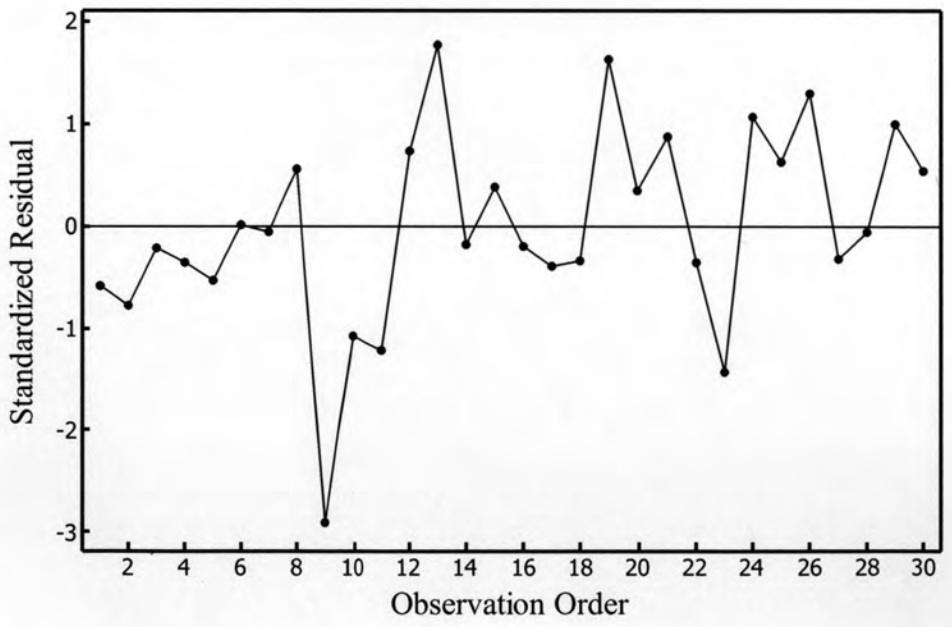

Figure 4.12 Standardized residual and run order plot of 2,4-DCP degradation.

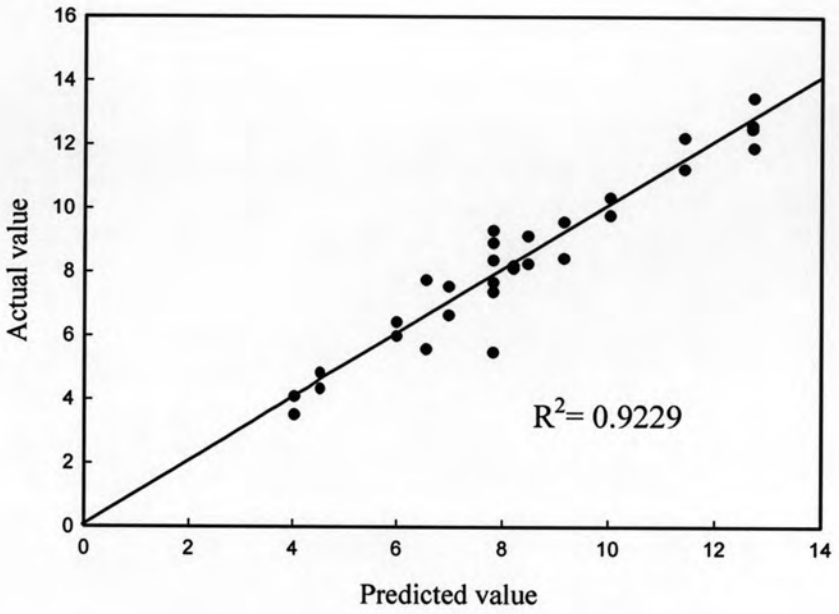

Figure 4.13 Plot of actual and predicted values

Table 4.5 Estimated regression coefficients for % 2,4-DCP degradation

Term	Coef.	Std. error of Coef.	*p*-value
Constant	7.8387	0.3649	<0.001 *
Type of template	-0.4762	0.2235	0.046
Catalyst loading	3.2199	0.2235	<0.001 *
%Fe	0.1345	0.2235	0.554
Template*Template	-0.8020	0.3289	0.129
Catalyst loading*Catalyst loading	0.4855	0.3289	0.024
mol %Fe* mol %Fe	1.1850	0.3289	0.156
Template * Catalyst loading	-0.2194	0.3160	0.002 *
Template * mol %Fe	0.6118	0.3160	0.67
Catalyst loading * mol %Fe	-0.1486	0.3160	0.643

* significant effect

The observed value is compared with the predicted value, calculated from the model in Figure 4.13. It can be seen that the regression value (R^2= 0.9229) is fairly well fitted with the observed values.

As illustrated in Table 4.5 the computed regression coefficients for the model along with their respective *p*-values are presented. The *p*-values used as a tool to check the significance of each of coefficients. It can also indicate the pattern of interactions between the variables. A smaller value of *p* was more significant to the corresponding coefficient. Conventionally, higher 95% ($p < 0.05$) indicates the significance effect of the corresponding factors on the response. According to *p*-values, it can be concluded that the effects of catalyst loading and template type have significant on this model. However, *p*-value of template type (0.046) was close to 0.05. The effect of template type was concluded as low significance. The mathematical relationship between the parameters in the terms of polynomial equation is listed below (Equation 4.1).

$$\begin{aligned}\text{Conversion \%} = {} & 7.8387 - (0.4762 \times \text{Template}) + (3.2199 \times \text{Loading}) + \\ & (0.1345 \times \text{mol\%Fe}) - 0.8020 \times (\text{Template})^2 + 0.4855 \times \\ & (\text{Loading})^2 + 1.1850 \times (\text{mol\%Fe})^2 - 0.2194 \times (\text{Template x} \\ & \text{Loading}) + 0.6118 \times (\text{Template x mol\%Fe}) - 0.1486 \times \\ & (\text{Loading x mol\%Fe}) \qquad (4.1)\end{aligned}$$

In this work, the value of R^2 is evaluated to 0.9229. The value was reasonably sufficient to predict the further responses. However, if all insignificant effects in equation 4.1 were ignored, the adjusted determination coefficient (R^2_{adj}) became 0.8882. Those effects were interaction between type of template and type of template, mol% Fe and mol% Fe, type of template and mol% Fe, catalyst loading and mol% Fe.

The results of analysis of variance (ANOVA) are shown in Table 4.6 ANOVA is used to indicate the significance and adequacy of the model. The Fischer's F test (*F*-value) is measure of how well the factors describe the variation in the data about its mean. Normally, the value should be higher than 4.0 ($F>4.0$). *F* ratios are given by the ratio of sum square regression to sum square residual error. The *F* ratio from this

experiment is 11.97. It can be concluded that the model was sufficient significantly for 2,4-DCP degradation.

Table 4.6 ANOVA results for % degradation of 2,4-DCP

Source	Degree of freedom	Sequential sum of square	*F*-value	*p*-value
Regression	9	191.223	26.59	0.000
Linear	3	169.802	70.84	0.000
Square	3	17.865	7.45	0.002
Interaction	3	3.556	1.48	0.249
Residual Error	20	15.981		
Lack of Fit	3	0.613	0.23	0.877
Pure Error	17	15.368		
Total	29	207.04		

*R-squared = 92.29%; R-squared (adjust) = 88.82%

The main effect plot and interaction plot of the factors on the response variable are shown in Figure 4.14 The results presented that the 2,4-DCP degradation with different types of templates were not different from each other. This result correlated with BET surface area, where the template was not significant to the surface area. It might be the template was not completely removed in the calcinations method at 400°C to obtain the only anatase phase of TiO_2. From TG-DTA analysis, almost templates were removed at 600°C while, at this temperature, the anatase was transformed to rutile phase.

The efficiency of 2,4-DCP degradation trended to be increase when increasing the catalyst loading, due to the specific area of reaction was increased with more catalyst loading and enhanced the reaction between the photocatalyst and pollutant.

In this work, the amount of Fe Doping on N-TiO_2 presented no interaction effect to the 2,4-DCP degradation. It may be the small amount of Fe was not enough to completely disperse on high surface area of catalyst.

(a)

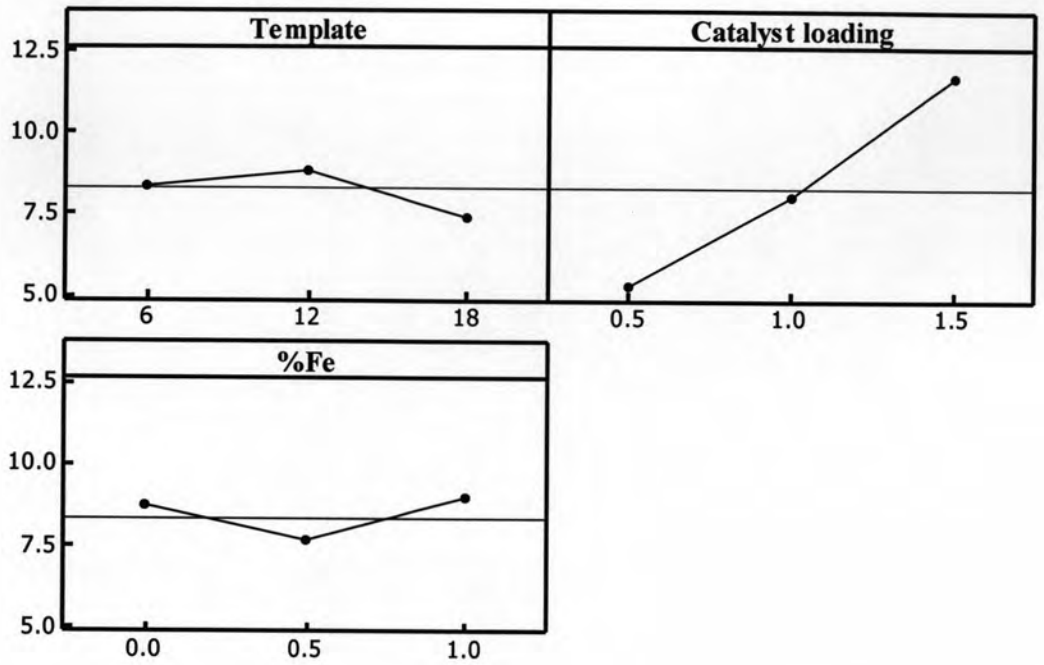

(b)

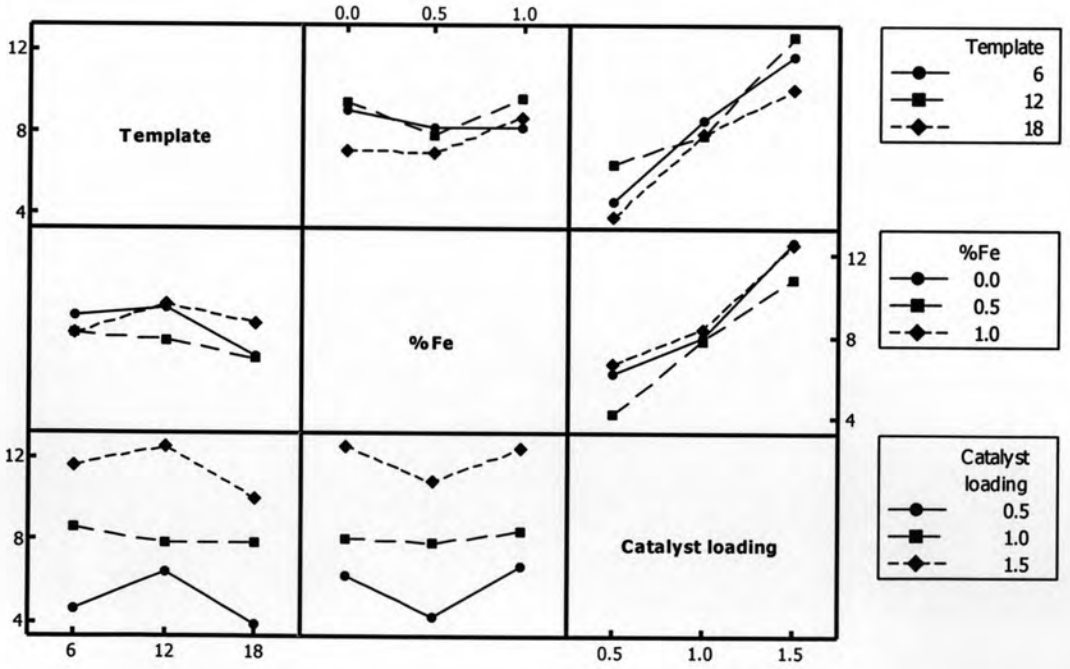

Figure 4.14 Main effect plots (a) and interaction plots (b) on 2,4 DCP degradation

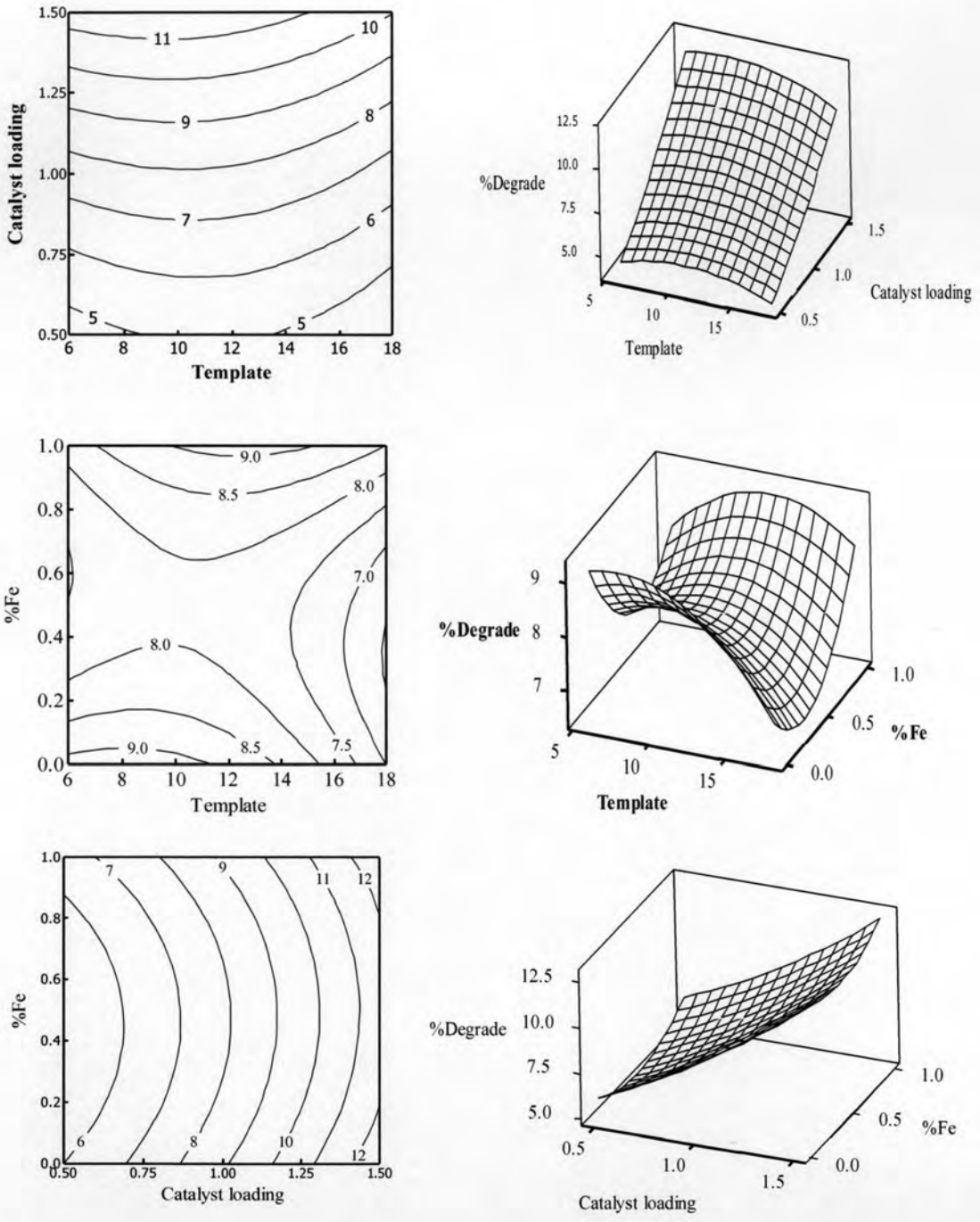

Figure 4.15 Contour plots and surface plots on studied parameters.

(a) Template type and Catalyst loading

(b) Template type and Fe content

(c) Catalyst loading and Fe content

The response surfaces and contour graphs. The surfaces and contours plot are given in Figure 4.15. It provided a simple method to optimize the efficiency of the treatment and contributed to the identification of the interactions between the factors.

The effect of template type and catalyst loading is presented in Figure 4.15(a). The high degradation efficiency was captured at the region of catalyst loading (1.25-1.5 g/L), and template type between 6C to 10C. The data presented in Figure 4.15(b) is described the relation between template type and Fe content. The plot indicates that the template type between 6C to10C is more efficiency with no Fe content. Strong evidence of interaction between catalyst loading and Fe content is shown in Figure 4.15(c). The high efficiency of 2,4-DCP degradation was performed with catalyst loading in rang of 1.25-1.5 g/L and no Fe content.

From the Box-Behnken analysis, the optimal operating condition was selected to apply of 0.0 mol% Fe doping, 6C template type, and the catalyst loading of 1.5 g/L.

4.2.2 Kinetic study

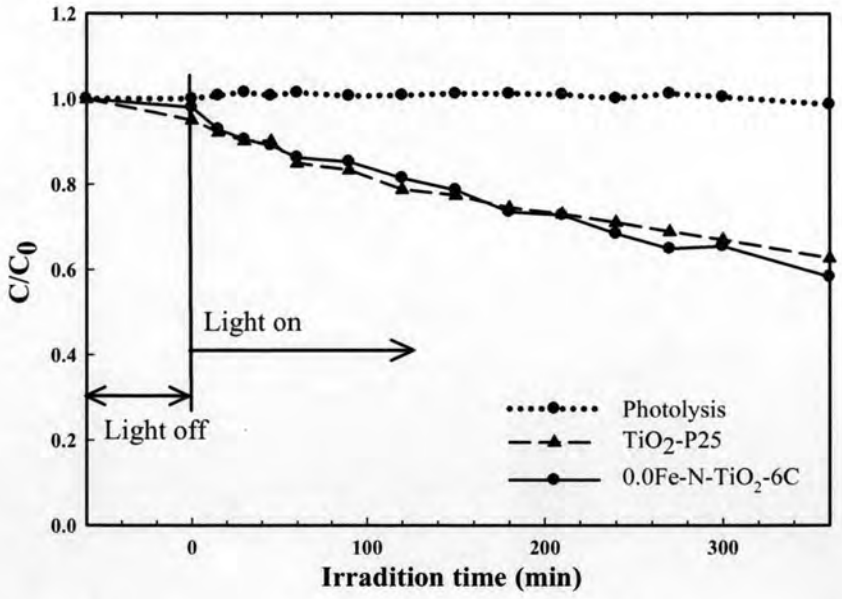

Figure 4.16 Concentration change of 2,4-DCP under various condition (Control parameter: 15 ppm of 2,4-DCP, 1.5 g/L of catalyst, pH 5.5, 6 h)

This experiment was investigated at pH 5.5 that nearly to the pH_{zpc} of TiO_2-P25. Under visible range of light, referring to photolysis, the degradation of 2,4-DCP was less than 2.0% within 6 h without catalyst. It, therefore, can imply that light alone cannot degrade 2-4,DCP in any range of wavelength. The comparison tests were carried out on both P25 and 0.0Fe-N-TiO_2-6C photocatalysts. However, before photocatalysis took place, an adsorption phenomenon has been performed for 1 h. There was little adsorption taken place in light-off region, assuming that adsorption did not dominate the degradation. The result showed that performance on both catalysts (P25 and 0.0Fe-N-TiO_2) was somewhat equally. The degradation was about 40% within 6 h.

The degradation efficiency for different 2,4-DCP concentrations is shown in Figure 4.17. It was found that initial concentration of 5 ppm provided the highest reduction. The reduction was about the same (ca. 35-40%) at higher concentration, starting from 10 ppm.

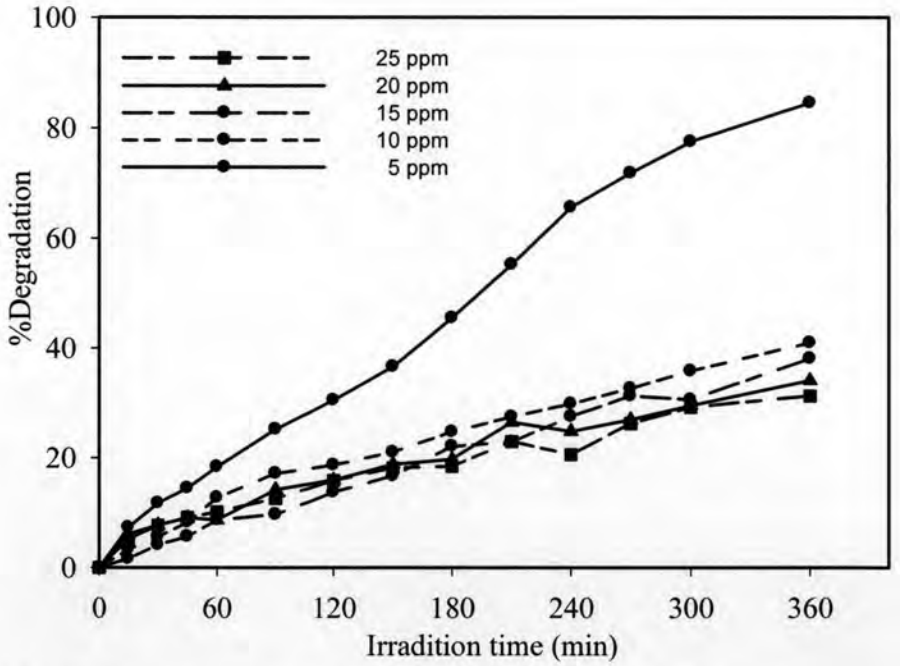

Figure 4.17 Concentration change of 2,4-DCP of 0.0Fe-N-TiO_2-6C at different initial concentration (Condition: 1.5 g/L of catalyst, pH 5.5, 6 h)

Because of the slow decay of 2,4 DCP and it could not complete degradation within 6 h. Since the immediate would be produced with time on stream, which caused the complexity of the whole reaction consideration. Therefore, kinetic analysis was conducted only at the first hour of experiment. The effects of initial concentrations within 1 h is showed in Figure 4.18

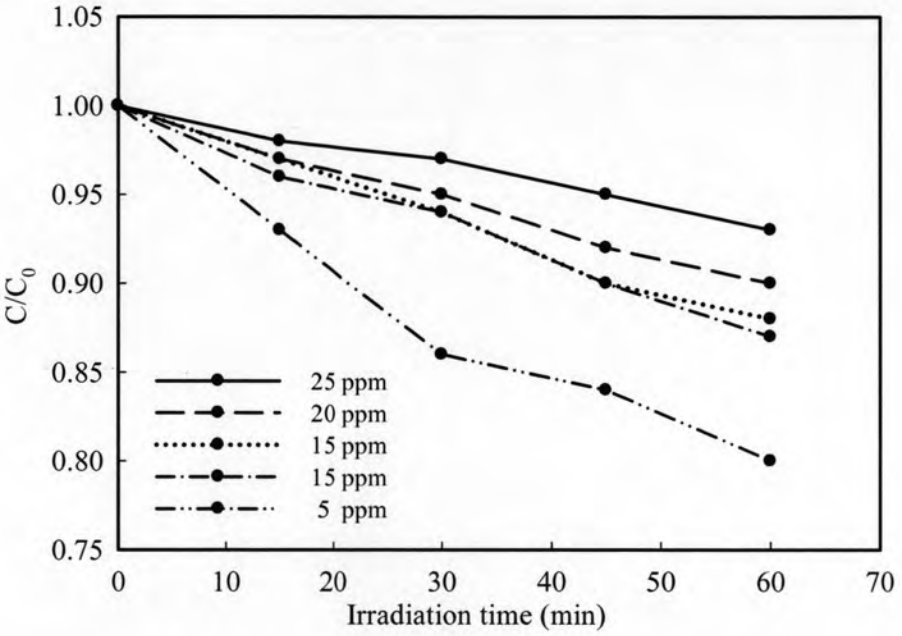

Figure 4.18 Initial concentration effect of 2,4-DCP
(Condition: 1.5 g/L of catalyst, pH 5.5, 1 h)

Initial rate method: This method is generally used to determine the rate expression. Assuming that A presents 2,4 DCP which will be decomposed or degraded to other intermediates (B), as follows (Fogler, 2006);

$$A \rightleftharpoons B$$

The rate of reaction can be expressed;

$$-r_A = k_f C_A^{\,n} - k_b C_B^{\,m} \qquad (4.2)$$

At an initial condition, product (B) concentration was assumed to be zero. The reaction rate should be followed zero order kinetic.

$$-\frac{dC}{dt}\Bigg| = k_f C_{Ao}^{n} \quad (4.3)$$

The "n" value in equation 4.3 was now set to zero. After the integration of equation 4.3 based on zero order, the equation result as follow;

$$C_A - C_{Ao} = kt \quad (4.4)$$

To determine kinetic parameters of k_f (forward rate constant) the plots of C_A-C_{Ao} versus t for each initial concentration was carried out and presented in Table 4.7.

Table 4.7 Rate constant o different initial concentrations.

Initial concentrations (ppm)	k	R^2
5	0.0163	0.9558
10	0.0213	0.9922
15	0.0310	0.9928
20	0.0330	0.9952
25	0.0283	0.9897

In this case the reaction order was confirmed to be zero order. This refered that. There was too much active site available. Therefore, the concentration of 2,4-DCP showed no effect to the reactions.